

Prepared by NASA
Agenda Item: WGII/8
Discussed in WGII

LIMB CORRECTION OF POLAR-ORBITING IMAGERY FOR THE IMPROVED INTERPRETATION OF RGB COMPOSITES

In response to CGMS action A43.12

Gary J. Jedlovec
NASA Marshall Space Flight Center, Huntsville, AL USA

Nicholas Elmer
University of Alabama in Huntsville, Huntsville, AL USA

Executive summary:

Red-Green-Blue (RGB) composite imagery combines information from several spectral channels into one image to aid in the operational analysis of atmospheric processes. However, infrared channels are adversely affected by the limb effect, the result of an increase in optical path length of the absorbing atmosphere between the satellite and the earth as viewing zenith angle increases. This paper reviews a newly developed technique to quickly correct for limb effects in both clear and cloudy regions using latitudinally and seasonally varying limb correction coefficients for real-time applications. These limb correction coefficients account for the increase in optical path length in order to produce limb-corrected RGB composites. The improved utility of a limb-corrected Air Mass RGB composite from the application of this approach is demonstrated using Aqua Moderate Resolution Imaging Spectroradiometer (MODIS) imagery. However, the limb correction can be applied to any polar-orbiting sensor infrared channels, provided the proper limb correction coefficients are calculated. Corrected RGB composites provide multiple advantages over uncorrected RGB composites, including increased confidence in the interpretation of RGB features, improved situational awareness for operational forecasters, and the ability to use RGB composites from multiple sensors jointly to increase the temporal frequency of observations.

Limb Correction of Polar-orbiting Imagery for the Improved Interpretation of RGB Composites

1 INTRODUCTION

This working paper is in response to CGMS action A43.12 from Working Group II “NASA to report on polar-based RGB composite viewing angle corrections to CGMS-44.” Current multispectral and hyperspectral satellite sensors incorporate channels in both visible and infrared (IR) wavelengths to gather useful information about atmospheric and surface conditions. Operational forecasters rely heavily on satellite data in their decision-making process, but have very limited time dedicated to interpreting satellite imagery. Therefore, with an increasingly vast amount of imagery available, it will be difficult for forecasters to use the information from all of these channels operationally. Red-Green-Blue (RGB) composites address this issue and aid the operational forecast community by combining information from several channels into one composite image. RGB composites are typically designed to address a specific forecast problem, such as identifying general air mass characteristics, airborne dust, or low-level clouds and fog, and therefore contain more qualitative information than single channel imagery alone. RGB composites allow forecasters to quickly gather the information they need, enhancing their situational awareness and enabling them to make decisions in a more efficient and timely manner. However, the interpretation of RGB composites derived from polar orbiting or geostationary satellite imagery can be problematic, particularly at large scan or view angles because of the increased atmospheric absorption in individual channels away from nadir viewing.

A suite of RGB composites are currently derived from polar-orbiting satellite sensors, such as Terra/Aqua Moderate Resolution Imaging Spectrometer (MODIS) and Suomi-NPP Visible Infrared Imaging Radiometer Suite (VIIRS), to provide global, high spatial resolution products as complementary products to similar lower resolution geostationary products (Jedlovec 2013; Fuell et al. 2016; and Zavodsky et al. 2013). Unfortunately, due to orbit characteristics and viewing geometries, IR imagery is significantly and adversely affected by an atmospheric effect known as limb-cooling (or limb-darkening in earlier literature; Wark 1962; Lienesch and Wark 1967). The limb effect typically causes anomalous cooling up to 4-11 K at the edge of the satellite swath (Goldberg et al. 2001; Liu et al. 2007), resulting in features on the limb appearing colder than if they were observed at nadir. When IR channels are combined into a RGB composite, the limb effect significantly impacts the resulting colors and therefore prevents the correct interpretation of atmospheric features at increasing scan angles away from nadir, leading forecasters and other product users to interpret these features with very low confidence, or even misinterpret the features altogether. As a result, RGB composites created from IR channels not corrected for limb effects can only be reliably interpreted close to nadir, which further reduces the coverage of an already temporally and spatially limited product. Therefore, to fully exploit the advantages of RGB composites derived from polar-orbiters, it is

necessary to correct the individual IR channels for limb effects prior to creating the composites.

2 LIMB CORRECTION METHODOLOGY

The limb correction methodology used in this research is presented in the recent publication by the authors (Elmer et al. 2016) and is briefly described below. The approach is largely based on previous studies and tuned to support RGB applications, particularly those derived from polar-orbiters. Earlier studies (e.g., Soden and Bretherton 1993, 1996; Joyce and Arkin 1997; Joyce et al. 2001) calculated the change in brightness temperature (BT) from nadir to the limb using collocated geostationary satellite pairs. They then used the linear best fit parameters between the change in BT and the natural logarithm of the cosine of θ_z (hereafter referred to as the θ_z -BT relationship) as limb correction coefficients to correct IR imagery as a function of θ_z . Instead of using collocated satellite pairs to develop a θ_z -BT relationship, this research used top of atmosphere (TOA) radiances that were simulated for satellite sensors at varying θ_z using the Joint Center for Satellite Data Assimilation (JCSDA) Community Radiative Transfer Model (CRTM; Han et al. 2006) in order to increase sample size.

The CRTM forward model simulates TOA radiances for operational satellite sensors at various θ_z based on user-provided surface conditions and atmospheric profiles of temperature, water vapor, ozone, and other trace gases. For this study, surface skin temperature and profiles of temperature, ozone mass mixing ratio, and specific humidity were acquired from the European Center for Medium-Range Weather Forecasting (ECMWF; Dee et al. 2011) global reanalysis (ERA-Interim; ECMWF 2015). To limit the number of profiles processed in CRTM and ensure that only profiles representative of clear scenes were selected, a subset of cloud-free ECMWF profiles from March 2013 through February 2014 were processed in CRTM. These were selected using a 15° latitude by 15° longitude grid, in which a maximum of five cloud-free profiles, determined from the ERA-Interim total cloud cover parameter, were randomly selected from each grid box for each month. For grid boxes with less than five cloud-free profiles in a month, all cloud-free profiles were selected. This approach resulted in a total of 12,657 cloud-free profiles which represented the seasonal and latitudinal variations of temperature, water vapor, and ozone in the atmosphere. These 12,657 profiles were further separated based on surface type into land (3670) and water (8987) profiles. As a result, a wide range of possible surface and atmospheric conditions were represented in this study.

The CRTM atmospheric layers were defined by the 60 pressure levels of the ECMWF profiles. The model atmosphere was defined to be cloud- and aerosol-free with water vapor and ozone as absorbers. For each profile, simulations were completed at several θ_z (referred to as the sensor zenith angle in the model), ranging from 0° to 60° in 10° intervals. All other model geometry angles used the default values, including the source (solar) zenith angle of 100° (below the horizon) to remove solar reflection and isolate only the thermal component of the 3.9 μm shortwave window channel. Once the CRTM structures were properly defined, simulations were completed for each ECMWF profile for the range of θ_z previously

specified (0° to 60° in 10° intervals), from which BT and layer optical depth were retrieved for the relevant IR channels from MODIS.

Limb correction coefficients, which account for the increasing optical path length, were derived separately for each sensor channel based on the CRTM simulated radiances, which were converted to BT for the following analysis. For each sensor channel, CRTM BTs (T_{CRTM}), were binned by latitude (15° intervals) and month to account for latitudinal and seasonal variability, but longitudinal variability was ignored, similar to Joyce et al. (2001). The quadratic equation,

$$T_{\theta_z} - T_{\theta} = C_2 |\ln(\cos \theta_z)|^2 + C_1 |\ln(\cos \theta_z)|,$$

was used to describe the θ_z -BT relationship, where T_0 is the T_{CRTM} at nadir, T_{θ_z} is the T_{CRTM} at θ_z , and the quadratic best fit parameters, C_2 and C_1 , are defined as the limb correction coefficients, which vary latitudinally and seasonally. The r^2 correlation for band 27 (6.7 μm) was greater than 0.96. When the results were further separated by month, the r^2 correlation increased to nearly 0.99, indicating that the spread was primarily due to seasonal variability. Note that C_2 was approximately zero, indicating that the θ_z -BT relationship for absorption bands is roughly linear, similar to the finding of Soden and Bretherton (1993, 1996). Although the r^2 correlation increased slightly when divided by month, a strong separation between land and water profiles still exists. The MODIS band 31 results are also similar to those for other IR window channels.

In cloudy regions, to account for cloud effects due to a decrease in optical path length, limb correction scaling factors (Q) were calculated from CRTM layer optical depth (τ_1) using the following equations:

$$t_l(p) = e^{-\tau_1(p)}, \quad t(p) = t_l(p) t(p-1),$$

$$Q(p) = \frac{t(0) - t(p)}{t(0) - t(p_s)} = \frac{1.0 - t(p)}{1.0 - t(p_s)}$$

where $t_l(p)$ is the layer transmittance at pressure p , $t(p)$ is the total atmospheric transmission from pressure p to TOA, $t(0)$ is the transmittance at TOA, and $t(p_s)$ is the transmittance at the surface. Note that Q ranges between 0.0 (very high cloud detected) to 1.0 (no cloud detected). The above formulation assumes that clouds are opaque with an emissivity of 1.0, which is not the case for all clouds, but it provides an acceptable approximation for correcting for most cloud effects.

The limb correction coefficients and scaling factors calculated using the above methodology were applied through the equation

$$T_{\text{CORR}} = T_B - T_{\text{OFFSET}} + Q \left(C_2 (\phi, \delta) \ln(\cos \theta_z)^2 - C_1 (\phi, \delta) \ln(\cos \theta_z) \right)$$

to correct swaths of IR imagery for limb effects. In the above equation, T_{CORR} is the limb-corrected brightness temperature, T_B is the sensor measured brightness temperature, and $C_1(\phi, \delta)$ and $C_2(\phi, \delta)$ are the channel specific limb correction

coefficients as a function of latitude (ϕ) and Julian day (δ). The T_{OFFSET} term adjusts for channel spectral differences between sensors on the various satellites (Elmer et al. 2016). Since the magnitude of the limb correction depends on the term $\ln(\cos\theta_z)$, a 10% change in the magnitude of the limb correction coefficients results in a change in T_{CORR} at $\theta_z=65^\circ$ (edge of MODIS swath) of less than 0.7 K for all IR window channels, 1.0 K for the water vapor absorption channels, and 1.5 K for the ozone absorption channel. If the limb correction coefficients were calculated only with respect to latitude by using an annual mean, errors in the limb correction coefficients would relate to changes in the T_{CORR} at $\theta_z=65^\circ$ of 1.0 K for IR window channels to as much as 3.5 K for water vapor and ozone absorption channels. Therefore, to avoid these errors, seasonal variations were accounted for in the calculation of the limb correction coefficients.

3 RESULTS

The results of applying the above methodology to IR imagery to correct for limb effects and examples demonstrating the improved interpretation of limb-corrected RGB composites are presented in this section. Validation of the limb correction algorithm was accomplished by comparing the limb-corrected IR imagery and RGB composites from polar-orbiters to the appropriate reference sensor for validation at shared near-nadir points. Limb effects are negligible for geostationary sensors near the nadir point, so geostationary time-coincident imagery can be used to validate the limb correction of RGB composites from polar-orbiting sensors.

Figure 1 compares uncorrected and corrected Aqua MODIS band 27 (6.7 μm) water vapor imagery to the corresponding SEVIRI band 5 (6.2 μm) water vapor imagery. Since water vapor is a major atmospheric absorber, the uncorrected Aqua MODIS image (Fig. 1b) shows significant limb-cooling, resulting in noticeable temperature differences of several Kelvin between Aqua MODIS and SEVIRI in both clear and cloudy regions. On the other hand, the corrected Aqua MODIS image (Fig. 1c) closely matches SEVIRI to the extent that many features appear identical and a smooth transition exists. Note, minor temporal differences contribute to some discontinuity between the scenes.

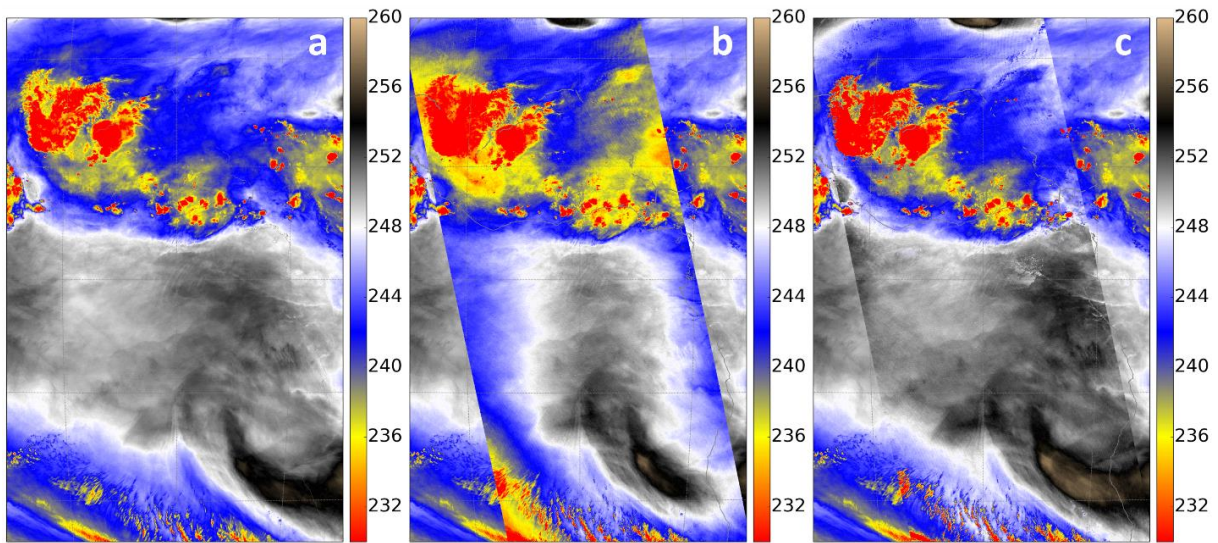


Figure 1. 1330 UTC 28 June 2015 (a) SEVIRI band 5 (6.2 μm) brightness temperatures (K) overlaid with (b) uncorrected and (c) corrected (limb and cloud effects) Aqua MODIS band 27 (6.7 μm) brightness temperatures (K).

A more quantitative comparison is presented in Figure 2a-b, which shows the brightness temperature difference (BTD) between the Aqua MODIS and SEVIRI images from Figure 1. The uncorrected Aqua MODIS image is 6-8 K cooler than SEVIRI on the limb (Fig. 2a), but roughly equal at nadir. The difference between the corrected Aqua MODIS image and SEVIRI is less than 2 K across the majority of the image, except for cloudy regions (Fig. 2b). Here, cloud movement, emissivity differences between wavelengths, and viewing geometries increase the absolute error. Note that in both images, the southern portion of the image indicates that Aqua MODIS is 2-3 K warmer than SEVIRI. This is evidence of limb-cooling in SEVIRI, which increases from the equator poleward.

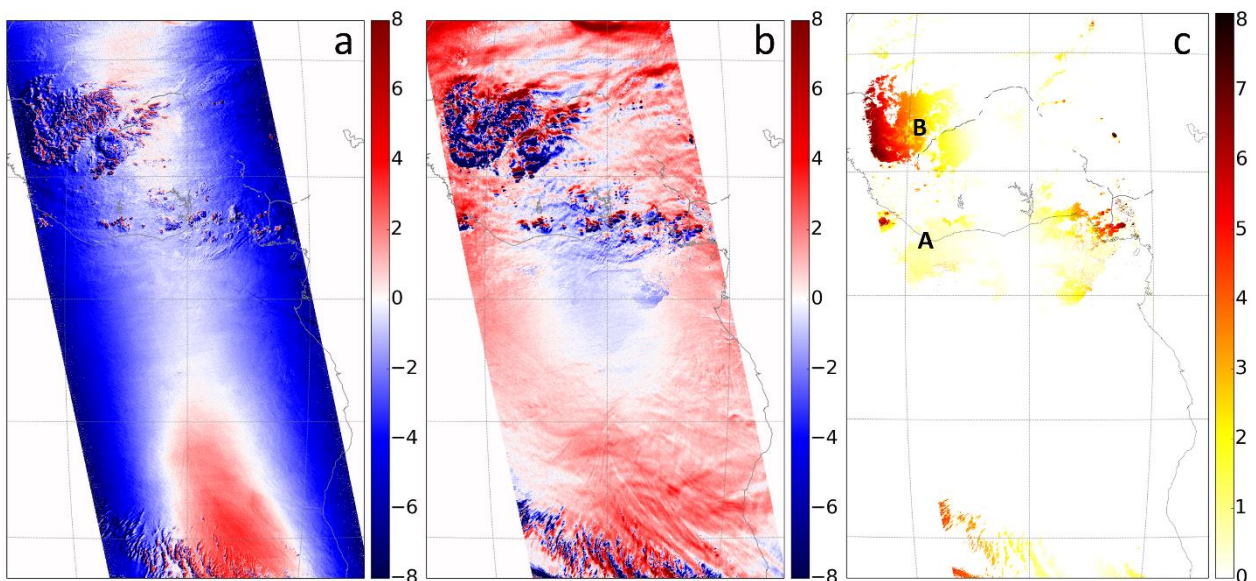


Figure 2. 1330 UTC 28 June 2015 BTD between the Aqua MODIS and SEVIRI bands from Figure 1. (a) Figure 1b minus 1a, (b) Figure 1c minus 1a, and (c)

Figure 1c minus the corrected (limb effects only) Aqua MODIS band 27 (not shown) BTD (K).

To demonstrate the importance of accounting for cloud effects, Figure 2c shows the BTD between the corrected (limb and cloud effects) Aqua MODIS band 27 (Fig. 1c) and the corrected (limb effects only) Aqua MODIS band 27 (not shown), hereafter referred to as the cloud effect difference (CED). Note that the only differences occur in cloudy regions, as expected. The stratus clouds along the coast (A) are low clouds and only cause a small decrease in the optical path length compared to a clear scene, resulting in a small CED of approximately 1 K. On the other hand, the cumulonimbus clouds over West Africa (B) result in a CED of 4-7 K, since they have higher cloud tops and therefore cause a greater reduction in the optical path length compared to the stratus clouds. Even though the cloud top pressure is likely similar across the cumulonimbus clouds, the CED clearly increases from 4 K to 7 K as θ_z increases. Therefore, even if cloud top pressure remains constant, cloud effects still increase as θ_z increases, since the clouds obscure a larger portion of the optical path length at larger θ_z . Although not shown, similar results are observed in cloudy regions for other absorption channels and IR window channels. Since window channels can detect the surface and low clouds, cloud effects are more significant in these channels.

Limb-corrected RGB composites are created by combining limb-corrected IR channels using the appropriate RGB recipe. Since the Air Mass RGB uses water vapor and ozone absorption channels, the impact of limb-cooling on the interpretation of this product is appreciable. A comparison of the uncorrected and corrected Aqua MODIS Air Mass RGB with the corresponding SEVIRI Air Mass RGB from 1330 UTC 28 June 2015 is shown in Figure 3. The uncorrected Aqua MODIS Air Mass RGB (Fig. 3a) is impacted by significant limb-cooling and the RGB coloring on the limb is much different from the corresponding RGB coloring in the SEVIRI image (Fig. 3d). Use of uncorrected channels in the Air Mass RGB can alter the interpretation of significant thermodynamic characteristics. For example, the blue coloring at points A, B, and C of the Aqua MODIS swath could be indicative of upper-level moist air or simply be the result of limb-cooling. A similar effect can be seen for points D and E in regions lacking green coloring. These regions, where the red coloring dominates, are consistent with the presence of upper-level dry air. However, as before, the same color can be mimicked by limb effects, so the atmospheric conditions at these locations can only be interpreted with low confidence. The limb-corrected Aqua MODIS Air Mass RGB (Fig. 3b), which only corrects for limb effects (correction of cloud effects omitted), demonstrates a significant improvement over the uncorrected Aqua MODIS Air Mass RGB. Not only is the coloring more consistent with what is shown in the SEVIRI Air Mass RGB, but the interpretation of the RGB features is less ambiguous. However, since Fig. 3b has not been corrected for cloud effects, clouds on the limb, such as the mid-level stratus at point F and the convective clouds below point A, are noticeably greener than they appear in the SEVIRI Air Mass (Fig. 3d). When cloud effects are accounted for, as shown in Figure 3c, the clouds more closely match those in the SEVIRI Air Mass RGB.

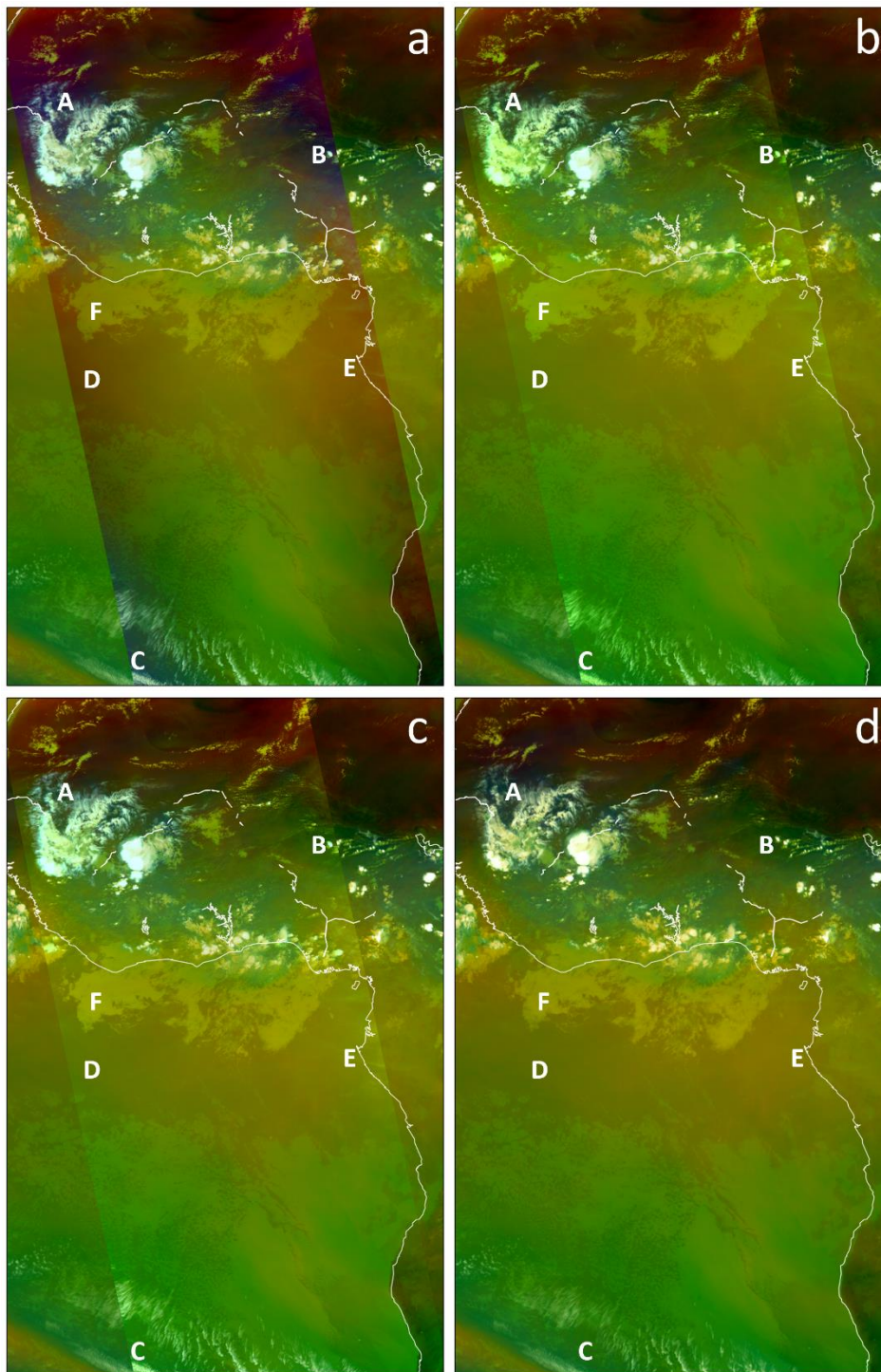


Figure 3. 1330 UTC 28 June 2015 (a) uncorrected, (b) corrected (limb effects only), and (c) corrected (limb and cloud effects) Aqua MODIS Air Mass RGB overlaying (d) the corresponding SEVIRI Air Mass RGB.

Similar results are seen when comparing Aqua MODIS to Advanced Himawari Imager (AHI) in the tropical pacific, indicating that the limb correction approach is virtually insensitive to longitudinal variations. Figure 4 compares the 1640 UTC 21 October 2015

uncorrected and corrected Aqua MODIS Air Mass RGB to the corresponding AHI Air Mass RGB. The uncorrected Aqua MODIS Air Mass RGB (Fig. 4a) shows significant limb-cooling, indicated by the lack of green coloring and widespread blue (A, C) and red (D, F) coloring along the edge of the swath. The blue component of the Air Mass RGB is strongest for cold brightness temperatures in the water vapor band. Blue is typically interpreted as a cold, polar air mass, but limb effects can create the same coloring. It can be difficult to determine whether the blue coloring indicates a cold, polar air mass or limb effects, especially at high latitudes where cold, polar air masses are prevalent. This particular example (Fig. 4) is near the equator, therefore

the likelihood that the blue coloring at points A and C indicate cold, polar air is low; however, the blue coloring does impede interpretation of the image. The coloring at locations D and F, which may indicate dry air, present a similar dilemma, since red coloring is clearly visible at nadir (E) as well as on the limb. The corrected Aqua MODIS Air Mass RGB (Fig. 4b) enables the proper interpretation, in which A and C are correctly interpreted as tropical air, whereas D and F are correctly interpreted as regions of subsidence.

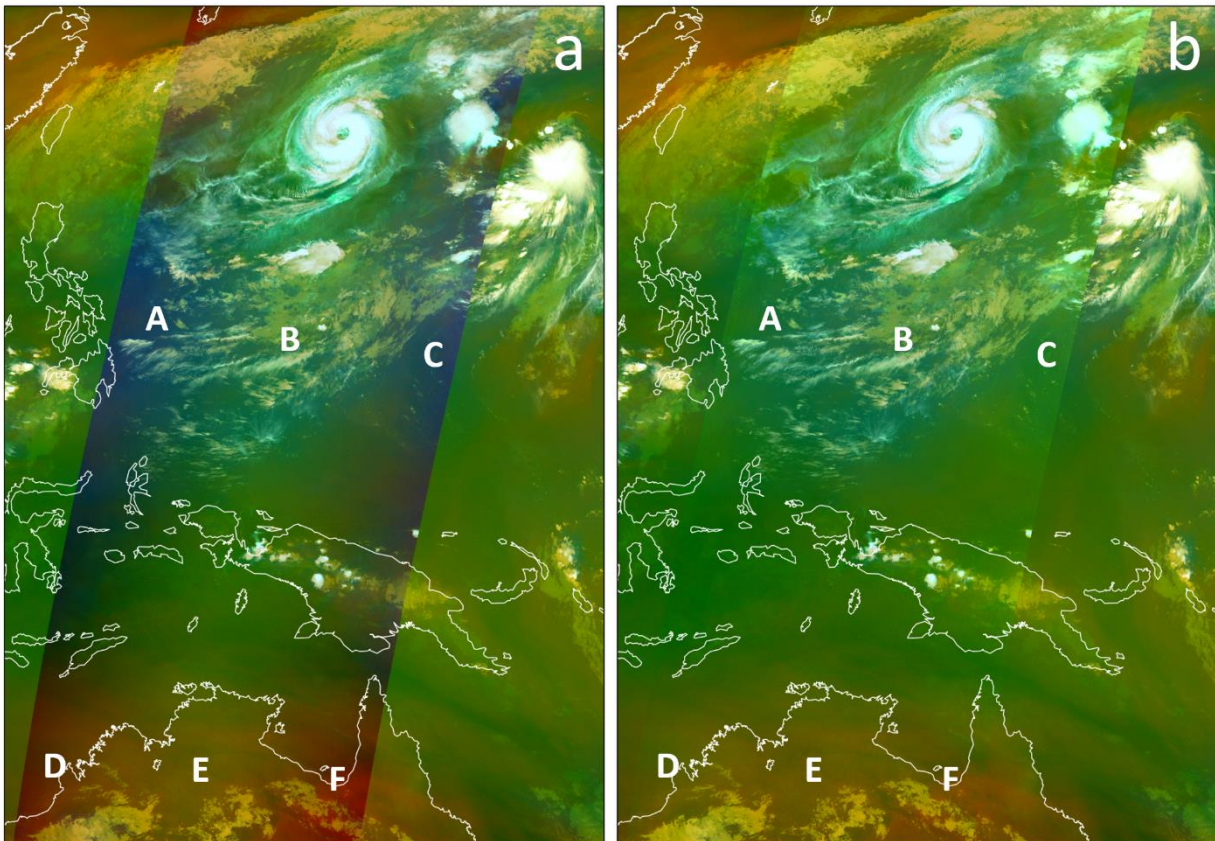


Figure 4. 1640 UTC 21 October 2015 (a) uncorrected and (b) corrected (limb and cloud effects) Aqua MODIS Air Mass RGB overlaying the corresponding AHI Air Mass RGB.

4 SUMMARY AND CONCLUSION

This study developed a correction methodology to remove limb effects in IR channels from polar-orbiters. Using CRTM simulated brightness temperatures, limb correction coefficients were derived as a function of latitude and season to account for the increase in optical path length with increasing θ_z . The limb correction approach was shown to greatly improve the interpretation of the RGB composites. The limb correction was most effective for the water vapor and ozone absorption channels, where significant limb-cooling was present in the uncorrected imagery. In general, limb effects resulted in anomalous cooling of 5-10 K on the limb in uncorrected water vapor/ozone channels, whereas 2-5 K of limb-cooling was observed in window channels. The limb correction reduced the anomalous cooling to 1-2 K for all

channels in both clear and cloudy regions. As a result, errors in BTs due to limb effects were significantly reduced.

It was shown that corrected RGB composites enable RGB features on the limb to be correctly interpreted with high confidence, since they more accurately represent atmospheric features. As a result, operational forecasters will have improved situational awareness and can produce more informed forecasts. Additionally, limb correction allows for the full RGB image to be utilized, no longer constraining the interpretation to near nadir points. This improves the spatial coverage of accurate RGB imagery, increases the number of useful observations, and enables RGB composites from multiple sensors to be used jointly to increase the temporal frequency of RGB imagery.

Even though the case example shown in this paper focused only on the limb correction of MODIS IR bands used to create the Air Mass composite, this limb correction methodology can be applied to any IR channel, even those on other polar-orbiting sensors, including AVHRR. Additionally, ongoing work includes developing a limb correction methodology suitable for geostationary sensors, such as SEVIRI, AHI, and the Advanced Baseline Imager (ABI), in order to improve the interpretation of RGB composites derived from these sensors at mid-latitudes.

MODIS and VIIRS RGB composites are currently being produced at NASA SPoRT in real-time and delivered to operational end users in the United States, including NOAA NWS forecast offices and National Centers (Jedlovec 2013). The correction is not computationally intensive, and therefore takes seconds to process a full swath of imagery. The limiting factor is the latency of the cloud product for the purpose of accounting for cloud effects. However, correcting only for limb effects and omitting the correction for cloud effects to maintain real-time processing still provides a significant improvement in RGB interpretation.

5 REFERENCES

- Dee, D. P. and Coauthors, 2011: The era-interim reanalysis: configuration and performance of the data assimilation system. *Quart. J. Roy. Meteor. Soc.*, 137, 553-597.
- ECMWF, 2015: ERA-Interim. <http://www.ecmwf.int/en/research/climate-reanalysis/era-interim>.
- Elmer, N. J., E. Berndt, and G. Jedlovec, 2016: Limb correction of MODIS and VIIRS infrared channels for the improved interpretation of RGB composites. *J. Atmos. Ocean. Technol.*, DOI: <http://dx.doi.org/10.1175/JTECH-D-15-0245.1>.
- Fuell, K. K., B. J. Guyer, D. Kann, A. L. Molthan, and N. Elmer, 2016: Next generation satellite RGB dust imagery leads to operational changes at NWS Albuquerque. *J. Operational Meteor.*, 4 (6), 75–91.
- Goldberg, M. D., D. S. Crosby, and L. Zhou, 2001: The limb adjustment of AMSU-A observations: Methodology and validation. *J. Appl. Meteor.*, 40, 70-83.
- Han, Y., P. van Delst, Q. Liu, F. Weng, B. Yan, R. Treadon, and J. Derber, 2006: JCSDA Community Radiative Transfer Model (CRTM). Tech. rep., Washington, D.C.

- Jedlovec, G., 2013: Transitioning research satellite data to the operational weather community: The SPoRT Paradigm. *IEEE Geo. Rem. Sens. Mag.*, 1 (1), 62-66, doi:10.1109/MGRS.2013.2244704.
- Joyce, R. and P. A. Arkin, 1997: Improved estimates of tropical and subtropical precipitation using the GOES precipitation index. *J. Atmos. Oceanic Technol.*, 14, 997-1011.
- Joyce, R., J. Janowiak, and G. Huffman, 2001: Latitudinally and seasonally dependent zenith-angle corrections for geostationary satellite IR brightness temperatures. *J. Appl. Meteor.*, 40, 689-703.
- Lienesch, J. H. and D. Q. Wark, 1967: Infrared limb darkening of the Earth from statistical analysis of TIROS data. *J. Appl. Meteor.*, 6, 674-682.
- Liu, Q. and F. Weng, 2007: Uses of NOAA-16 and -18 satellite measurements for verifying the limb-correction algorithm. *J. Appl. Meteor. Climatol.*, 46, 544-548.
- Soden, B. J., and F. P. Bretherton, 1993: Upper tropospheric relative humidity from the GOES 6.7 μm channel: Method and climatology for July 1987. *J. Geophys. Res.*, 98 (D9), 16 669-16 688.
- Soden, B. J., and F. P. Bretherton, 1996: Interpretation of TOVS water vapor radiances in terms of layer-average relative humidities: Method and climatology for the upper, middle, and lower troposphere. *J. Geophys. Res.*, 101 (D5), 9333-9343.
- Wark, D. Q., 1993: Adjustment of TIROS Operational Vertical Sounder data to a vertical view. Tech. rep., Washington, D.C.
- Zavodsky, B. T., A. L. Molthan, and M. J. Folmer, 2013: Multispectral imagery for detecting stratospheric air intrusions associated with mid-latitude cyclones. *J. Operational Meteor.*, 1 (7), 71-83, doi:10.15191/nwajom.2013.0107.